catalysts

MDPI

Article

Highly Efficient and Selective Oxidation of Benzyl Alcohol by WO_4^{2-} Catalyst Immobilized by a Phosphonium-Containing Porous Aromatic Framework

Bingxin You [1], Zeliang Cheng [2], Yuyang Tian [2], Shaolei Wang [2,*] and Baolin Wang [2,*]

[1] Center of Disease Immunity and Intervention, College of Medicine, Lishui University, Lishui 323000, China; youbx634@nenu.edu.cn
[2] Key Laboratory of Polyoxometalate and Reticular Material Chemistry of the Ministry of Education, Faculty of Chemistry, Northeast Normal University, Changchun 130024, China; chengzl968@nenu.edu.cn (Z.C.); tianyy100@nenu.edu.cn (Y.T.)
* Correspondence: wangsl030@nenu.edu.cn (S.W.); wangbl296@nenu.edu.cn (B.W.)

Abstract: Benzoic acid has found a wide range of applications in the chemical industry. The selective oxidation of benzyl alcohol is one of the main routes to produce benzoic acid. In this work, *tris*(4-bromobiphenyl)phosphine was chosen as a building block to synthesize PAF-181 with a high specific surface area and high yield via a Yamamoto–Ullmann reductive coupling reaction. Subsequently, the WO_4@PAF-181 catalyst was successfully prepared via methylation and ion exchange, in which PAF-181 acts as a carrier while WO_4^{2-} serves as the active catalytic site. The synergistic effect between functional carriers and active sites endows WO_4@PAF-181 with distinctive catalytic property for efficient selective oxidation of benzyl alcohol to benzoic acid. Importantly, the catalyst can be conveniently recovered and reused by simple filtration, still maintaining its high catalytic activity.

Keywords: porous aromatic frameworks; selective oxidation; benzoic acid

Citation: You, B.; Cheng, Z.; Tian, Y.; Wang, S.; Wang, B. Highly Efficient and Selective Oxidation of Benzyl Alcohol by WO_4^{2-} Catalyst Immobilized by a Phosphonium-Containing Porous Aromatic Framework. *Catalysts* **2023**, *13*, 1309. https://doi.org/10.3390/catal13091309

Academic Editor: Jorge Bedia

Received: 3 August 2023
Revised: 18 September 2023
Accepted: 18 September 2023
Published: 20 September 2023

1. Introduction

Benzoic acid, as the simplest organic aromatic acid, finds extensive applications in the fields of medicine, food, and the chemical industry [1,2]. It also serves as a pivotal precursor in the organic synthesis industry [3]. Recent research indicates that electrocatalysis [4], photocatalysis [5], and chemical catalysis [6–17] have been extensively investigated for the purpose of selectively oxidizing benzyl alcohol. Particularly, there has been significant scholarly interest in exploring the selective oxidation of benzyl alcohol through chemical catalysis. Oxidizing agents such as $KMnO_4$ [6], CrO_3 [7], and iodosobenzene [8] have been employed in existing research, but often lead to substantial production of pollutants. To address these concerns, alternative oxidants including O_2 [9,10], H_2O_2 [11–13], potassium peroxymonosulfate (Oxone) [14,15], and *tert*-butyl hydroperoxide (*t*-BuOOH) [16,17] have been utilized for the efficient synthesis of benzoic acid. Moreover, various transition metals have been investigated as catalysts for the selective oxidation of alcohols to carboxylic acids. Notably, noble metal catalysts such as gold, palladium, and iridium have exhibited remarkable catalytic activity in this regard [18–21].

Recently, porous organic polymers (POPs) have gained significant attention and emerged as promising catalyst supports in the field of organic catalysis due to their exceptional characteristics, including high specific surface area, excellent stability, and facile post-modification capabilities [22,23]. In 2017, Huang successfully synthesized a series of imidazole-containing crosslinked POPs (poly(divinylbenzene-co-*N*-vinylimidazole), PDVB-VI-n) via free-radical polymerization. Subsequently, these POPs were employed as supports for immobilizing gold nanoparticles (Au NPs), which were prepared through coordination of $AuCl_3$ and $NaBH_4$ reduction, exhibiting good activity for the heterogeneous catalysis of

the aerobic oxidation of benzyl alcohol [1]. Furthermore, in 2019, Loh installed Au NPs and Ag NPs onto the surface of thiol-functionalized block copolymer particles, achieving the first interfacial gold- and silver-catalyzed aerobic oxidation of benzyl alcohol to benzoic acid [24]. However, it should be noted that metal NPs are susceptible to agglomeration and deactivation during the reaction [25]. Additionally, the preparation of POPs through free-radical polymerization presents challenges in terms of process control, resulting in relatively random product structures. Moreover, the use of metal catalysts may lead to contamination of the final product [26–28].

Porous aromatic frameworks (PAFs) represent a novel category of POPs. These frameworks consist of structural units derived from aromatic rings, which are interconnected by robust carbon–carbon covalent bonds formed via straightforward organic coupling reactions [29]. The pore structure of PAFs can be tailored through the topological design of monomers, and the aromatic monomers can also be easily pre-modified and post-modified to achieve desired functionality [30]. Furthermore, PAFs exhibit not only high specific surface area but also exceptional chemical and thermal stability under harsh conditions, such as elevated temperatures, strong acids and alkalis, and various organic solvents. These remarkable properties render PAFs promising candidates as supports for heterogeneous catalysts [31]. Given the advantages of PAFs and the significance of benzoic acid, our objective is to develop cost-effective, recyclable, and environmentally benign catalysts by strategically designing the framework structure to enable the green and sustainable synthesis of benzoic acid.

Herein, we intend to develop the strategy to immobilize inexpensive metal ions into PAFs to prepare heterogeneous catalysts that enhance their selective catalytic efficiency for the oxidation of benzyl alcohol to benzoic acid. PAF-181 is designed and synthesized through Ullmann coupling of *tris*(4-bromobiphenyl)phosphine [29] as a heterogeneous catalyst platform on the basis of the following considerations: (i) the employment of long-sized biphenyl units easily creates larger pore volumes, providing enough space for the introduction of the subsequent active centers and the accommodation of organic substrates; (ii) the electron-donating nature of the phosphine center (P III) enables facile coordination with transition metals; (iii) phosphine can be oxidized to phosphonium cations (P V), thereby constructing a cationic framework for convenient modification [32,33]. Given the enhanced stability of high-valence P in ambient conditions, we employed methyl iodide to oxidize the P center in PAF-181 to phosphonium cations by a methylation reaction, leading to the successful synthesis of I@PAF-181. Subsequently, we conducted an anion ion exchange using low-cost sodium tungstate to replace I^- in I@PAF-181 [34]. Finally, the target catalyst WO_4@PAF-181 was successfully obtained, which was further used to catalyze the selective green oxidation of benzyl alcohol (Scheme 1).

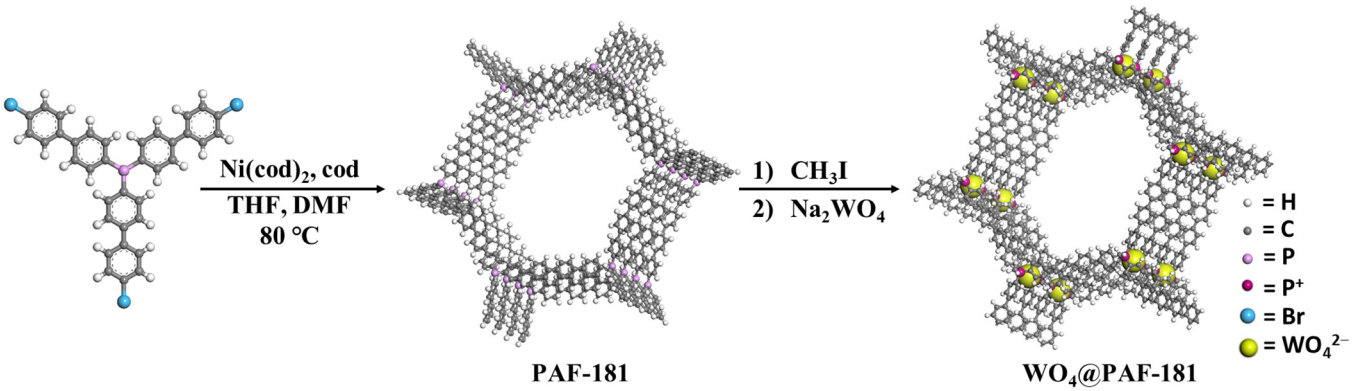

Scheme 1. The synthetic route of PAFs and their theoretical model.

2. Results

2.1. Structural Characterization

The structure of the materials was systematically investigated through a series of characterization techniques. Fourier transform infrared (FT-IR) spectroscopy (Figure 1a) was employed to characterize the structure and composition of PAF-181 and its building blocks. It was observed that the C–Br stretching vibration absorption peak at 518 cm^{-1} (curve I) in the fingerprint region vanished in curve II, proving the successful synthesis of PAF-181. Following the methylation reaction, I@PAF-181 exhibited a saturated C–H stretching vibration absorption peak at 2800–3000 cm^{-1} (curve III), indicating the successful installation of methyl groups. The comparison between WO_4@PAF-181 and I@PAF-181 revealed that WO_4@PAF-181 displayed a stretching vibration absorption peak of W–O at 841 cm^{-1} in curve IV, signifying the effective immobilization of WO_4^{2-} anions within the porous framework.

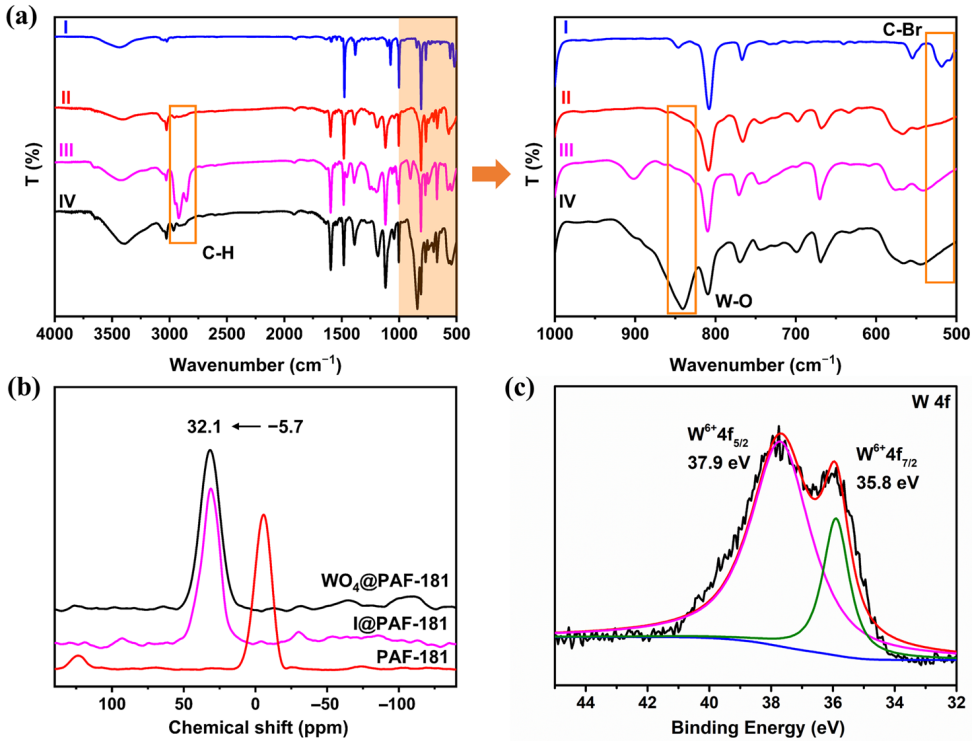

Figure 1. FT-IR and ^{31}P CP/MAS solid-state NMR spectra of the PAFs and XPS fine spectra of W 4f for WO_4@PAF-181: (**a**) FT-IR spectra of tris(4-bromobiphenyl)phosphine (I, blue), PAF-181 (II, red), I@PAF-181 (III, magenta), and WO_4@PAF-181 (IV, black); (**b**) ^{31}P solid-state NMR of PAF-181 (red), I@PAF-181 (magenta), and WO_4@PAF-181 (black); (**c**) peak fitting of W 4f spectrum for WO_4@PAF-181.

Powder X-ray diffraction (PXRD) was performed to investigate the crystallinity of PAF-181, I@PAF-181, and WO_4@PAF-181 (see Figure S1a). The results show that the three PAFs all exhibit an amorphous nature. Notably, the absence of diffraction peaks corresponding to Na_2WO_4 or tungsten oxide in WO_4@PAF-181 suggests a homogeneous dispersion of W species within the material's pores, predominantly in the ionic form of WO_4^{2-}.

The ^{13}C cross-polarization/magic angle spinning (CP/MAS) solid-state nuclear magnetic resonance (NMR) spectrum of PAF-181 (see Figure S2) indicated the presence of aromatic carbon signal peaks at 139 and 126 ppm. In the spectra of I@PAF-181 and WO_4@PAF-181, an additional peak of aliphatic carbon was observed at 30 ppm, which can be attributed to the methyl carbon bonded to phosphorus, thereby confirming the methylation of P(III). However, it should be noted that the methyl carbon peak in the WO_4@PAF-181 NMR spectrum appeared relatively weak due to the signal-to-noise ratio of solid-state NMR and

the influence of WO_4^{2-} on the carbon spectrum. Furthermore, the ^{31}P CP/MAS solid-state NMR analysis of PAF-181 (Figure 1b) demonstrated a signal peak for P(III) at −5.7 ppm, while the P(V) signal peaks for I@PAF-181 and WO_4@PAF-181 were observed at 32.1 ppm. The aforementioned characterization results provide evidence for the successful synthesis of the desired products.

The morphological characteristics of the materials were examined using scanning electron microscopy (SEM). As shown in Figure S3, the three PAFs are all composed of small particles partially bonded together, albeit with slight morphological variations. PAF-181 displays numerous irregular small particles and partially spherical-like particles of varying sizes adhered together, resulting in a relatively rough particle surface. After methylation, the particles in I@PAF-181 demonstrate enhanced uniformity and a smoother surface. WO_4@PAF-181 showcases more approximately spherical particles that are uniformly distributed throughout the image. The transmission electron microscope (TEM) mapping images (see Figure S4) reveal that the elements of PAF-181 (C, P), I@PAF-181 (C, P, I), and WO_4@PAF-181 (C, P, O, W) are uniformly distributed throughout the frameworks. Furthermore, the absence of I in the WO_4@PAF-181 sample proves a relatively complete exchange of I^- for WO_4^{2-} ions. X-ray photoelectron spectroscopy (XPS) (Figures 1c and S5) also confirms the successful loading of WO_4^{2-} onto the WO_4@PAF-181 framework. The binding energies of 35.8 eV and 37.9 eV are attributed to the $W^{6+}4f_{7/2}$ and $W^{6+}4f_{5/2}$ orbital characteristics of WO_4^{2-}, respectively. An inductively coupled plasma atomic emission spectroscopy (ICP-AES) test demonstrates that the P content in PAF-181 is 5.8 wt%, which closely aligns with the theoretical content of 6.3 wt%. Additionally, the P and W contents in WO_4@PAF-181 are 4.1 wt% and 14.1 wt% (see Table S1), respectively, which are also in agreement with the theoretical contents (P: 4.9 wt%, W: 14.6 wt%).

The thermal stability of the materials was assessed using a thermogravimetric analyzer (TGA) in an air atmosphere. It was observed that PAF-181 (Figure 2a) exhibited favorable thermal stability, with significant framework collapse occurring at approximately 456 °C. However, a new inflection point emerged around 533 °C, potentially attributable to the oxidation of the P element on the framework to form P_2O_5. Following the methylation, the removal of free I^- in I@PAF-181 resulted in a weight loss of nearly 20% within the temperature range of 200–400 °C [35]. After ion exchange, WO_4@PAF-181 still retained high thermal stability, with framework collapse occurring around 456 °C. Furthermore, a minor weight loss in the low-temperature region (<200 °C) was observed, which can be attributed to the desorption of water molecules absorbed by the ionic material [35]. The W content determined from the combustion residual mass fraction of WO_3 (17.5 wt%) was found to be 13.8 wt%, consistent with the ICP-AES analysis result.

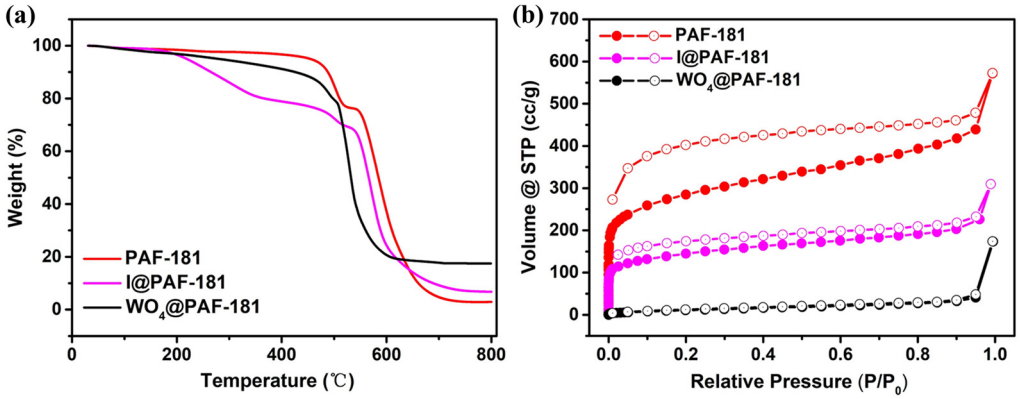

Figure 2. Thermogravimetric and N_2 physical sorption characterization of the PAFs: (**a**) TGA plots of PAF-181, I@PAF-181, and WO_4@PAF-181; (**b**) N_2 adsorption–desorption isotherms at 77 K for PAF-181, I@PAF-181, and WO_4@PAF-181.

The catalytic performance of POPs is heavily influenced by their pore structure [36]. To further analyze the pore structures of PAF-181, I@PAF-181, and WO_4@PAF-181, N_2

physical sorption at 77 K was conducted and their pore characteristics (see Table S2) were obtained based on the corresponding isotherms (Figure 2b). PAF-181 and I@PAF-181 exhibit a type I isotherm with steep adsorption at low pressures of $P/P_0 \leq 0.01$, which is a typical characteristic of surface coverage in porous materials, indicating the presence of micropores in the framework. The hysteresis loop observed between the adsorption and desorption branches of the isotherms across the entire relative pressure range suggests the existence of inner framework mesopores with uneven sizes or outer particle–particle large pores [37]. Methylation results in a significant reduction in the adsorption capacity of I@PAF-181 at low pressure due to the occupation of pores by -CH_3 and I^-. In general, both PAFs can be classified as microporous–mesoporous composite materials. However, the adsorption capacity of WO_4@PAF-181 decreases sharply at low pressure (P/P_0 = 0.01, 3.8 cc/g), but increases exponentially as pressure rises. This overall trend indicates a type III isotherm, suggesting that larger WO_4^{2-} ions occupy most of the micropores after ion exchange, leading to a significant increase in the ratio of mesopores and macropores. This result is consistent with the pore volume information obtained from the adsorption–desorption isotherms.

According to Brunauer–Emmett–Teller (BET) theory, surface areas of 1029, 579, and 45 $m^2\ g^{-1}$ are obtained for PAF-181, I@PAF-181, and WO_4@PAF-181, respectively. The surface area decreases significantly as the size of the modified functional group increases. The pore size distributions calculated by the quenched solid density functional theory (QSDFT) with the lowest fitting-error principle show the main pore sizes of 1.27 nm and 1.19 nm for PAF-181 and I@PAF-181, respectively (see Figure S6). And their mean pore diameters are 3.44 nm and 3.54 nm, respectively. The exchange of WO_4^{2-} results in a significant increase in the mean pore diameter (24.1 nm) for WO_4@PAF-181, despite the main pore size of 1.83 nm (micropore range). Consequently, there is a substantial reduction in the proportion of micropores, while mesopores dominate. Nonetheless, a significant quantity of preserved mesopores is sufficient to offer space for subsequent chemical reactions.

The water wetting properties of the materials were measured using a water contact angle meter (see Figure S7). The water contact angle of PAF-181 was measured to be 130°, indicating its hydrophobic nature. Following the methylation reaction, the water contact angle decreased to 93°, suggesting a significant enhancement in the hydrophilicity of I@PAF-181. After ion exchange, the contact angle of WO_4@PAF-181 was found to be 88°, signifying its hydrophilic nature. The inherent hydrophilicity of WO_4@PAF-181 facilitates its effective dispersion in aqueous media, thereby enhancing its interaction with water-soluble reactants.

2.2. Catalytic Performance

After conducting a comprehensive investigation on the structural characterization of WO_4@PAF-181, the catalytic behavior towards the oxidation of benzyl alcohol by H_2O_2 was explored [38–40]. The optimization of the reaction conditions was investigated. The corresponding results are presented in Table 1. It is observed that the presence of acid significantly influences the reaction outcome. In the absence of acid (Table 1, entry 1), the reaction yield is notably low (13%). Consequently, various common acids such as tartaric acid, *p*-toluenesulfonic acid (TsOH), and $NaHSO_4$ (Table 1, entries 2, 3, 11) were screened. The yield of benzoic acid gradually increased with the acidity level of the employed acid. This finding is consistent with the relevant literature [41], which indicates that a benzaldehyde intermediate is formed during the oxidation process of benzyl alcohol to benzoic acid. The resultant benzaldehyde undergoes a hydration balance in an acidic environment and will be partially converted to acetal, which can generate benzoic acid via α-H elimination. Therefore, the enhanced acidity of the system is advantageous for promoting benzoic acid formation, which also aligns with the experimental yields. It is important to note that the utilization of 1 mol% $NaHSO_4$ (99%) leads to higher yields compared to the use of 0.5 mol% (53%) (Table 1, entries 4 and 11). The absence of a catalyst resulted in a low

yield (26%, Table 1, entry 5), underscoring the essential role of a catalyst in achieving a high yield of benzoic acid. Furthermore, comparative experiments were conducted employing various catalysts (Table 1, entries 6, 7, 8, and 11). Entries 6 and 7 demonstrate that PAF-181 and I@PAF-181 exhibit limited catalytic activity, while WO_4^{2-} demonstrates good catalytic activity (Table 1, entry 8). And entry 11 reveals that WO_4@PAF-181 exhibits superior catalytic activity (99% yield) compared to PAF-181, I@PAF-181, and WO_4^{2-}. The limited activity of PAF-181 and I@PAF-181 may be ascribed to the acceleration of the decomposition of H_2O_2, resulting in lower yields compared to the catalytic system containing WO_4^{2-} [42]. Additionally, due to its poor solubility in water, benzyl alcohol tends to accumulate on the surface and pores of WO_4@PAF-181 through hydrophobic interaction, thereby increasing its contact probability with catalytic active sites. The synergistic effect between the support material and the catalytically active sites enhances the conversion efficiency of benzyl alcohol. Furthermore, to exclude the potential oxidation impact of WO_4^{2-}, a control experiment was conducted without the addition of H_2O_2 and no product was observed (Table 1, entry 9), indicating that H_2O_2 served as the oxygen source for the reaction. It is noteworthy that the addition of 4 mmol H_2O_2 results in a higher yield compared to the addition of 3 mmol H_2O_2 (Table 1, entries 10 and 11). Subsequently, the optimal reaction temperature was also screened (Table 1, entries 11–13), revealing that an increase in temperature correlated positively with an increase in the yield of the desired product, with 110 °C being the preferred temperature. Based on these experimental results, the optimal conditions for this reaction were established (Table 1, entry 11), and the corresponding GC spectrum is shown in Figure S8. Importantly, when compared to the previously reported heterogeneous catalyst Au/NPC (benzoic acid yield: 60%) supported by noble metal NPs [43], it was observed that the WO_4@PAF-181 composite exhibited superior yields under identical conditions. These outcomes undoubtedly validate the exceptional catalytic activity and promising potential of WO_4@PAF-181 for environmentally friendly benzoic acid synthesis.

To investigate the applicability of the above catalytic reaction conditions to diverse substrates, a series of catalytic oxidation reactions involving substituted benzyl alcohols were examined, and the isolated yields of the corresponding benzoic acid derivatives were determined. The experimental results in Table 2 demonstrate that the presence of electron-donating groups (such as $–CH_3$ and $–OCH_3$) in the substituted benzyl alcohols result in enhanced catalytic activity of the catalyst, leading to the production of the desired aromatic acid with a yield exceeding 93%. However, when the benzyl alcohols contain substituents with halogen atoms (e.g., –F, –Cl, –Br) or electron-withdrawing groups (e.g., –CN), a slight decrease in yield (<7%) was observed. Nevertheless, a high yield (ranging from 89% to 93%) of the target product was still obtained. Overall, the impact of different substituents of the substrates on the reaction yield was found to be negligible.

Based on the relevant literature [44–46] and our experimental results, a plausible mechanism for the catalytic oxidation of benzyl alcohol by WO_4@PAF-181 is proposed (Figure 3). Initially, the W=O double bond of WO_4^{2-} reacts with H_2O_2 to form sodium peroxytungstate (I) [44]. Subsequently, benzyl alcohol enriched in the WO_4@PAF-181 matrix undergoes a reaction with sodium peroxytungstate (I) to yield intermediate (II), which next generates benzaldehyde through the α-H elimination [45]. Further oxidation of the C=O double bond of benzaldehyde occurs via H_2O_2, resulting in the formation of intermediate (III). Finally, benzoic acid is produced through α-H elimination [46]. Nevertheless, similar investigations have suggested that the oxidation reaction of peroxides may also involve a free-radical mechanism [47,48].

Recyclability serves as a distinctive characteristic of heterogeneous catalysts. To assess the recyclability of WO_4@PAF-181, ten catalytic cycles of the oxidation of benzyl alcohol were conducted, with the results presented in Figure 4. Remarkably, the yield of benzoic acid remained notably high (>90%) even after the completion of the tenth cycle and the TOF of the reaction also remains almost unchanged, thus attesting to no substantial decrease in the catalytic efficiency. Furthermore, the retrieval and restoration of

the catalyst can be readily achieved through a straightforward process involving filtration, ethanol washing, and subsequent vacuum drying at 100 °C for 12 h. These experiments demonstrate WO_4@PAF-181 is an excellent heterogeneous catalyst with good recyclability and selectivity.

Table 1. The control experiments for the oxidation reaction of benzyl alcohol catalyzed by WO_4@PAF-181 [a].

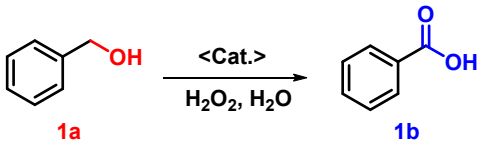

Entry	Catalyst	Acid	Temperature (°C)	T (h)	Yield (%) [b]
1	WO_4@PAF-181	None	110	24	13
2	WO_4@PAF-181	Tartaric acid	110	7	69
3	WO_4@PAF-181	TsOH	110	7	73
4 [c]	WO_4@PAF-181	$NaHSO_4$	110	7	53
5	None	$NaHSO_4$	110	7	26
6	PAF-181	$NaHSO_4$	110	7	10
7	I@PAF-181	$NaHSO_4$	110	7	16
8	Na_2WO_4	$NaHSO_4$	110	7	77
9 [d]	WO_4@PAF-181	$NaHSO_4$	110	7	0
10 [e]	WO_4@PAF-181	$NaHSO_4$	110	7	96
11	WO_4@PAF-181	$NaHSO_4$	110	7	99
12	WO_4@PAF-181	$NaHSO_4$	60	7	81
13	WO_4@PAF-181	$NaHSO_4$	r.t.	7	58

[a] Reaction conditions (unless otherwise noted): 1a (1.0 mmol), WO_4@PAF-181 (13.0 mg, 1 mol%), $NaHSO_4$ (1.0 mol%), 30% H_2O_2 (4.0 mmol) stirred in 4 mL H_2O at 110 °C for 7 h; [b] GC yield; [c] $NaHSO_4$ (0.5 mol%); [d] without H_2O_2; [e] H_2O_2 (3 mmol).

Table 2. Oxidation reactions of substituted benzyl alcohols catalyzed by WO_4@PAF-181 [a].

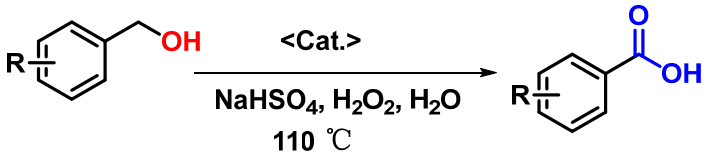

Entry	Substrates	Products	Yield (%) [b]
1	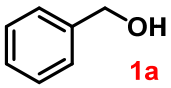	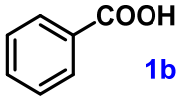	95
2	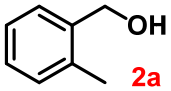	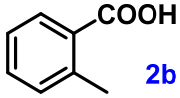	94
3	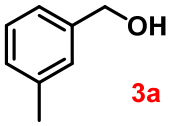	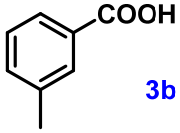	93

Table 2. *Cont.*

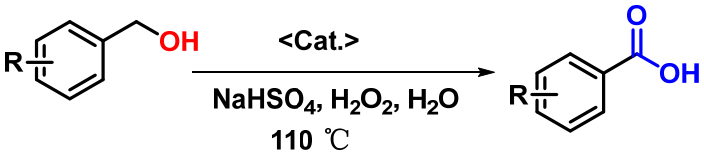

Entry	Substrates	Products	Yield (%) [b]
4	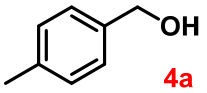	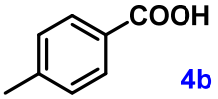	95
5	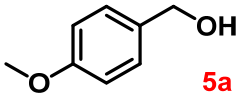	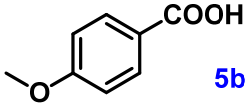	96
6	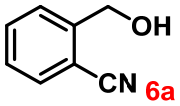	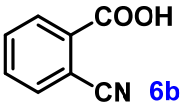	92
7	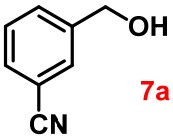	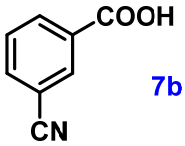	91
8	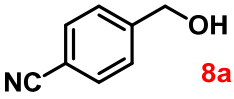	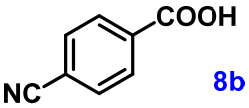	91
9	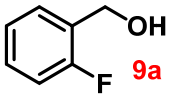	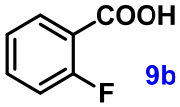	90
10	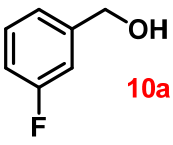	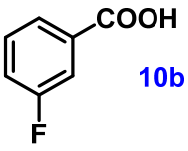	91
11	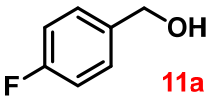	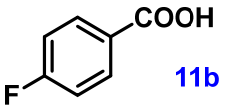	89
12	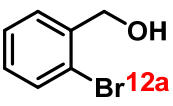	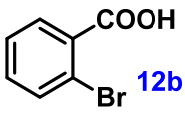	93
13	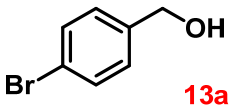	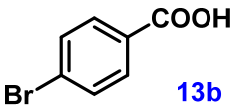	92
14	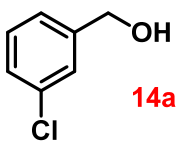	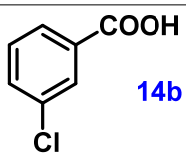	89

Table 2. *Cont.*

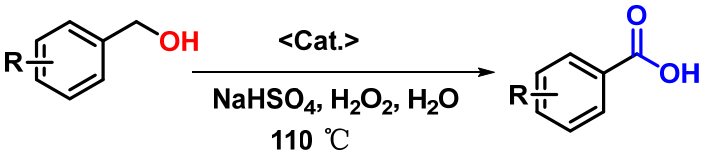

Entry	Substrates	Products	Yield (%) [b]
15	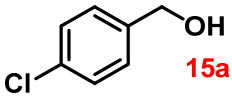 15a	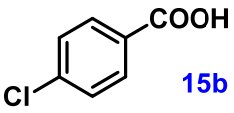 15b	91

[a] Reaction conditions (unless otherwise noted): 1a (1.0 mmol), WO_4@PAF-181 (13.0 mg), $NaHSO_4$ (1 mol%), 30% H_2O_2 (4.0 mmol) stirred in 4 mL H_2O at 110 °C for 7 h; [b] isolated yield.

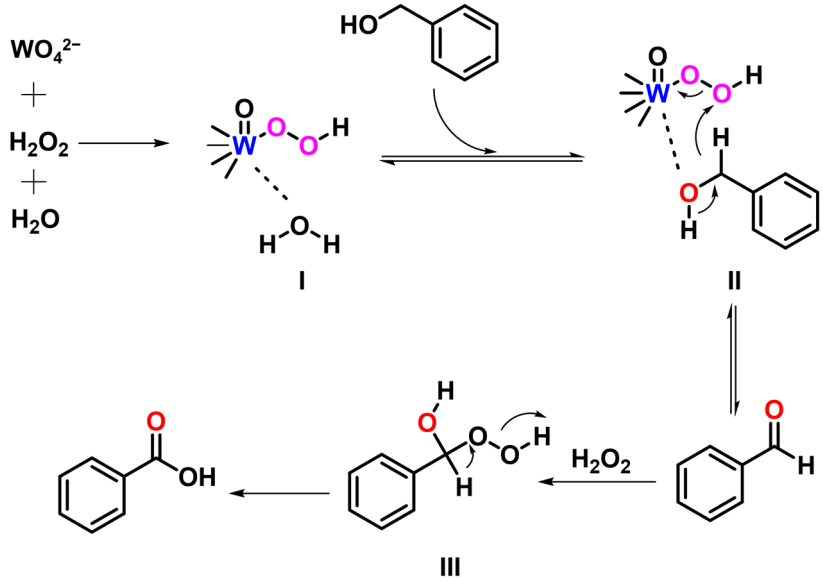

Figure 3. A possible mechanism diagram of the reaction.

In addition, we also studied the kinetics of the reaction (see Figure S9). The benzaldehyde concentration in the system underwent a progression from a lower level to a higher level and subsequently returned to a lower level, whereas the rate of increase in benzoic acid concentration initially exhibited a rapid rise followed by deceleration. This phenomenon could potentially be attributed to the initial abundance of oxidant content during the early phase of the reaction, followed by a gradual decline in concentration during the later stage of the reaction as well as dynamic equilibrium between two-step reactions.

Subsequently, the catalyst recovered after the tenth cycle was characterized using PXRD and FT-IR (see Figures S1b and S10) and it was found that the material framework remained unchanged. The SEM images (see Figure S11) also demonstrated that the recovered WO_4@PAF-181 maintained its original morphology. Furthermore, the contents of P and W in the recovered WO_4@PAF-181 were analyzed using ICP-AES and determined to be 4.0 wt% and 13.5 wt%, respectively (see Table S1), which are consistent with the initial WO_4@PAF-181, indicating almost no leaching of metallic species. Moreover, we have conducted a hot catalyst filtration (after 3.5 h, ca. 51.6% benzyl alcohol conversion). Following the implementation of hot filtration on the catalyst, an extended heating period failed to exhibit discernible transformation of benzyl alcohol and benzaldehyde within the filtrate (Figures S12 and S13). Subsequent analysis via ICP-AES further confirmed the absence of tungsten (W) in the filtrate (Table S1). The results indicate that tungsten did not leach and WO_4@PAF-181 is indeed a heterogeneous catalyst in nature. All of the

above investigations validate that the catalyst did not experience structural alterations, thus confirming the exceptional catalytic activity and robust stability of WO_4@PAF-181.

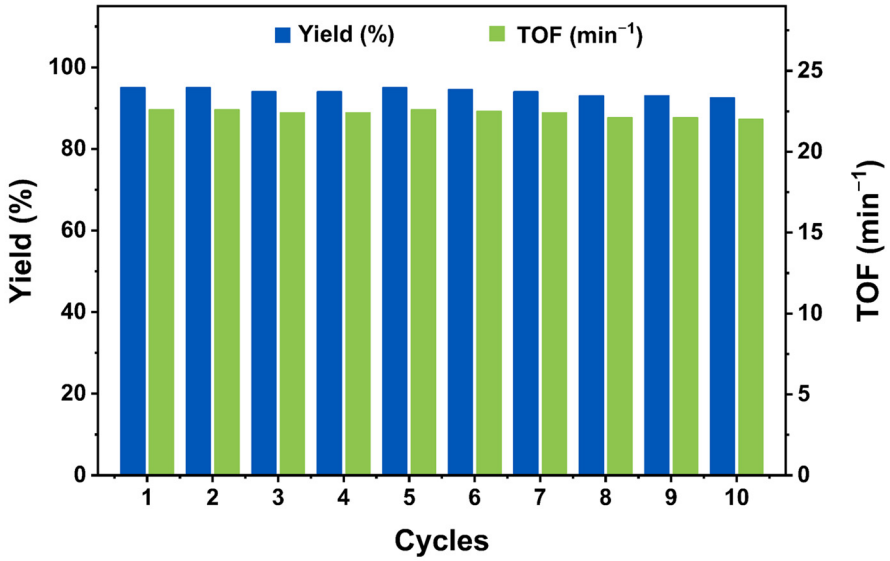

Figure 4. Recycling tests for WO_4@PAF-181 catalyst in the oxidation of benzyl alcohol (see the loop test for conditions). The blue column represents benzoic acid yield, and the green column represents TOF.

In the presence of various catalysts, the oxidation reactions of benzyl alcohol were compared, and the data summary is shown in Table 3.

Table 3. Oxidation of benzyl alcohol catalyzed by different catalysts.

Entry	Catalysts	Oxidant	Solvent	Yield (%)	Ref.
1	WO_4@PAF-181	H_2O_2	H_2O	99	this work
2	I@PAF-181	H_2O_2	H_2O	16	
3	PAF-181	H_2O_2	H_2O	10	
4	Na_2WO_4	H_2O_2	H_2O	77	
5	HPW/MCM-48	H_2O_2	H_2O	66	[49]
6	Au/PDVB-VI-n	O_2	H_2O	80	[1]
7	Au1–xAgx	O_2	H_2O	67	[50]
8	Au/Al_2O_3	O_2	EtOH	81	[51]
9	Au101/AC	O_2	EtOH	76	[52]
10	*p*-Co_3O_4	O_2	CH_3CN	30	[53]
11	Fe_3O_4@SiO_2-Schiff base-Co(II)	O_2	CH_3CN	91	[54]
12	Holey HEO	O_2	-	16	[55]
13	RPB-O_3	O_3	ethyl acetate	94	[56]

3. Materials and Methods

3.1. Synthesis of tris(4-bromobiphenyl)phosphine

To a 500 mL two-necked flask was added 4,4′-dibromobiphenyl (14.88 g, 48 mmol) and anhydrous THF (300 mL) under an N_2 atmosphere. The mixture was stirred at −78 °C for 20 min and *n*-BuLi (2.5 M, 19.4 mL, 48 mmol) was slowly added dropwise. After stirring for 2 h, a large pale-yellow precipitate appeared. Subsequently, PCl_3 (1.4 mL,

16 mmol) was added dropwise. The mixture was stirred at −78 °C for 1 h and slowly warmed to room temperature overnight. The reaction was quenched with saturated NaCl (100 mL), extracted with THF (100 mL × 3), dried over anhydrous Na_2SO_4, and the solvent was removed by rotatory evaporation to obtain the crude product. The crude product was purified using flash column chromatography using CH_2Cl_2 and petroleum ether (*v*:*v* = 1:4) as the eluent. The target product *tris*(4-bromobiphenyl)phosphine was obtained as a white solid. (3.5 g, yield: 30%). ^{1}H NMR (500 MHz, $CDCl_3$) δ 7.57–7.55 (m, 12H), 7.46–7.42 (m, 12H); ^{13}C NMR (126 MHz, $CDCl_3$) δ 140.47, 139.33, 136.39, 136.30, 134.41, 134.25, 132.01, 128.66, 127.13, 127.07, 121.98; ^{31}P NMR (202 MHz, $CDCl_3$) δ –7.38.

3.2. Synthesis of PAF-181

To a 100 mL flask was added $Ni(cod)_2$ (400 mg, 1.4 mmol), 2,2′-bipyridine (224 mg, 1.4 mmol), anhydrous DMF (6 mL), anhydrous THF (6 mL), and 1,5-cyclooctadiene (0.18 mL, 1.4 mmol) under an N_2 atmosphere. The mixture was stirred at 80 °C for 1 h, during which the mixture turned dark purple.

To a 25 mL one-neck flask was added *tris*(4-bromobiphenyl)phosphine (290 mg, 0.4 mmol), and anhydrous DMF (6 mL). Then, the mixture was preheated at 80 °C. After the white solid dissolved completely, the resulting solution was added into the above-mentioned mixture. The mixture was stirred at 80 °C for 24 h. Cooled to room temperature, the precipitate was filtered, washed with HCl (6 M, 200 mL × 3), H_2O (100 mL × 3), extracted with THF Soxhlet for 48 h, and dried under vacuum at 80 °C for 24 h (186 mg, yield: 95%).

3.3. Synthesis of WO_4@PAF-181

To a 25 mL double-necked flask was added PAF-181 (100 mg), and anhydrous CH_2Cl_2 (20 mL) under an N_2 atmosphere. The mixture was soaked in an ice-water bath for 20 min. CH_3I (0.2 mL) was added dropwise and then the reaction was stirred at room temperature for 24 h. Filtered and dried under vacuum at 80 °C for 24 h, the desired product (I@PAF-181) was obtained as a light-yellow solid powder (yield: 99%).

An I@PAF-181 (100 mg) and Na_2WO_4 solution (0.3 M, 20 mL) was added into a 50 mL beaker and the mixture was stirred at room temperature for 48 h. After filtration, the precipitate was washed with H_2O (50 mL × 3) and EtOH (50 mL × 3) and dried under vacuum at 80 °C for 24 h. WO_4@PAF-181 was obtained as a white solid powder (yield: 99%).

3.4. Catalytic Reaction

WO_4@PAF-181 (13 mg, WO_4^{2-}: 1 mol%) was added as a catalyst for the reaction in a 10 mL pressure-resistant tube. Subsequently, a magnetic stir bar, benzyl alcohol (104 μL, 1.0 mmol), 30% H_2O_2 (408 μL, 4.0 mmol, 4.0 eq.), $NaHSO_4$ (12 mg, 1 mol%, 0.01 eq.), and H_2O (4 mL) were added. The pressure-resistant tube was placed in an oil bath at 110 °C, and the reaction was stirred for 7 h. Cooled to room temperature, the organic phase was extracted with ethyl acetate (10 mL × 3), dried over anhydrous Na_2SO_4, and the solvent was removed using rotatory evaporation. Pure benzoic acid was obtained after recrystallization using ethyl acetate and petroleum ether.

3.5. Leaching Experiment

To a 25 mL single-neck flask, WO_4@PAF-181 (26 mg, WO_4^{2-}: 1 mol%), $NaHSO_4$ (24 mg, 1 mol%, 0.01 eq), benzyl alcohol (208 μL, 2.0 mmol), 30% H_2O_2 (816 μL, 8 mmol, 4.0 eq), H_2O (8 mL), and a magnetic stirrer was added. The mixture was sealed firmly with a rubber stopper and soaked in an oil bath at 110 °C. After stirring for 3.5 h, 0.2 mL of the filtrate was injected for GC analysis (see Figure S13). Then, a 30 mL glass sand core funnel was preheated in a 120 °C oven and the filtrate was quickly filtered into another 25 mL single-neck flask with a magnetic stirrer that had been previously placed in an oil bath at 110 °C. After further heating and stirring for 3.5 h, the mixture was cooled. A volume

of 0.2 mL of the filtrate was taken for GC analysis. A few drops of a mixed solution of hydrogen fluoride and nitric acid (*v*:*v* = 3:1) was added to the remaining filtrate to ensure the complete leak of the W species and full dissolution. The mixture was diluted to 25 mL in a plastic volumetric flask for the ICP-AES test (see Table S1) [57].

3.6. Loop Test

WO_4@PAF-181 (26 mg, WO_4^{2-}: 1 mol%) was added into a 25 mL pressure-resistant tube, and then a magnetic stirring bar, benzyl alcohol (204 µL, 2 mmol), 30% H_2O_2 (816 µL, 8.0 mmol, 4.0 eq.), $NaHSO_4$ (24 mg, 1 mol%, 0.01 eq.), and H_2O (8 mL) were added subsequently. The pressure-resistant tube was placed in an oil bath at 110 °C, and the reaction stirred for 7 h. Cooled down to room temperature, the precipitate was filtrated, washed with EtOH (30 mL × 3), and dried under vacuum at 80 °C for 12 h. It was noted there may be a very small amount of loss during the recovery, and therefore, the amount of recovered catalyst was reduced proportionally with respect to the amount of raw material. The above experiment was conducted 10 times.

4. Conclusions

In conclusion, considering the extensive utilization of benzoic acid in various domains of daily life and industrial production, a highly efficient and environmentally friendly heterogeneous catalyst was developed for the synthesis of benzoic acid. PAF-181, possessing abundant phosphorus centers, was successfully synthesized via a Yamamoto–Ullmann coupling reaction using *tris*(4-bromobiphenyl)phosphine as the reactive monomer. Subsequently, WO_4@PAF-181 was prepared through a methylation reaction and ion exchange. The catalytic performance of WO_4@PAF-181 on the selective oxidation of benzyl alcohol was investigated, employing H_2O_2 as the oxygen source and water as the reaction solvent. Remarkably high yields (89–96%) of benzoic acid and its derivatives were obtained. Furthermore, WO_4@PAF-181 exhibited superior catalytic activity compared to PAF-181, Na_2WO_4, and most other catalysts, thereby supporting the effectiveness of harnessing the synergistic effect between functionalized supports and active sites in constructing efficient heterogeneous catalysts. As a heterogeneous catalyst, WO_4@PAF-181 demonstrated excellent stability and recyclability, maintaining its high catalytic activity and selectivity after ten consecutive cycles. This study also highlights the significant potential applications of PAFs in organic synthesis.

Supplementary Materials: The following supporting information can be downloaded at: https://www.mdpi.com/article/10.3390/catal13091309/s1. Figure S1. Experimental PXRD patterns of PAF-181, I@PAF-181, WO_4@PAF-181 (a), $Na_2WO_4{\cdot}2H_2O$, fresh WO_4@PAF-181, and recycled WO_4@PAF-181 (b); Figure S2. ^{13}C CP/MAS solid-state NMR spectra of PAF-181, I@PAF-181, and WO_4@PAF-181; Figure S3. SEM images of PAF-181, I@PAF-181, and WO_4@PAF-181; Figure S4. TEM-EDX mapping images of PAF-181, I@PAF-181, and WO_4@PAF-181; Figure S5. XPS survey scan of WO_4@PAF-181; Figure S6. Pore size distributions of PAF-181, I@PAF-181, and WO_4@PAF-181; Figure S7. The water contact angles of PAF-181, I@PAF-181, and WO_4@PAF-181; Figure S8. GC spectrum of the standard mixed solution of ethyl acetate in equimolar amounts of benzyl alcohol, benzaldehyde, benzoic acid, and biphenyl (internal standard) (a), GC spectrum for the optimal reaction conditions (b); Figure S9. Plot of unconverted amount of benzyl alcohol and yield of benzaldehyde and benzoic acid vs. time during benzyl alcohol oxidation under optimal reaction conditions; Figure S10. FT-IR spectra of fresh WO_4@PAF-184 (I) and recycled WO_4@PAF-184 (II); Figure S11. SEM images of fresh WO_4@PAF-181 and recycled WO_4@PAF-181; Figure S12. Plot of benzyl alcohol conversion vs. time for the oxidation of benzyl alcohol, under the reaction conditions of entry 11, Table 1, in the presence of WO_4@PAF-181 (blue curve) and with filtering off the catalyst WO_4@PAF-181 after 3.5 h reaction time (orange curve); Figure S13. GC spectra of the filtrate at 3.5 h with WO_4@PAF-181 (a) and at 7 h without WO_4@PAF-181 (b) during the hot filtration test; Table S1. ICP-AES tests results for the P and W elements of PAF-181, fresh WO_4@PAF-181, recycled WO_4@PAF-181 (red font), and the filtrate after filtering off the catalyst WO_4@PAF-181 during the hot filtration test; Table S2. Characteristics of

pores in PAF-181, I@PAF-181, and WO_4@PAF-181 (calculated from their N_2 adsorption–desorption isotherms at 77 K using quenched solid density functional theory).

Author Contributions: Conceptualization, B.Y., S.W. and B.W.; methodology, B.Y.; validation, B.Y., Z.C. and B.W.; formal analysis, B.Y.; investigation, B.Y.; data curation, B.Y.; writing—original draft preparation, B.Y., Z.C., S.W. and B.W.; writing—review and editing, Y.T.; visualization, B.Y.; supervision, B.W.; project administration, B.W.; funding acquisition, B.W. All authors have read and agreed to the published version of the manuscript.

Funding: This research was funded by the Department of Science and Technology of Jilin Province, grant number 20220402028GH.

Data Availability Statement: The data presented in this study are available on request from the corresponding author.

Acknowledgments: The authors appreciate the support from Analytical and Testing Center of NENU for structural characterization.

Conflicts of Interest: The authors declare no conflict of interest.

References

1. Wang, H.; Shi, Y.; Haruta, M.; Huang, J. Aerobic oxidation of benzyl alcohol in water catalyzed by gold nanoparticles supported on imidazole containing crosslinked polymer. *Appl. Catal. A Gen.* **2017**, *536*, 27–34. [CrossRef]
2. Mao, X.; Yang, Q.; Chen, D.; Yu, B.; He, J. Benzoic acid used as food and feed additives can regulate gut functions. *BioMed Res. Int.* **2019**, *2019*, 5721585. [CrossRef] [PubMed]
3. Oktay, Y.; Leyla, G.; Ecem, A.; Saban, M.; Emel, A.; Ozer, K. Benzoic acid formation and its relationship with microbial properties in traditional Turkish cheese varieties. *Food Biosci.* **2021**, *41*, 101040. [CrossRef]
4. Xu, M.; Geng, J.; Xu, H.; Zhang, S.; Zhang, H. In situ construction of $NiCo_2O_4$ nanosheets on nickel foam for efficient electrocatalytic oxidation of benzyl alcohol. *Inorg. Chem. Front.* **2023**, *10*, 2053–2059. [CrossRef]
5. Zhang, S.; Wang, Y.; Ma, Y.; Li, Z.; Du, J.; Han, Z. Three-dimensional silver-containing polyoxotungstate frameworks for photocatalytic aerobic oxidation of benzyl alcohol. *Inorg. Chem.* **2022**, *61*, 20596–20607. [CrossRef] [PubMed]
6. Branko, J. Surfactant assisted permanganate oxidation of aromatic compounds. *Can. J. Chem.* **1989**, *67*, 1381–1383. [CrossRef]
7. Zhao, M.Z.; Li, J.; Song, Z.G.; Desmond, R.; Tschaen, D.M.; Grabowski, E.J.J.; Reider, R.J. A novel chromium trioxide catalyzed oxidation of primary alcohols to the carboxylic acids. *Tetrahedron Lett.* **1998**, *39*, 5323–5326. [CrossRef]
8. Tohma, H.; Takizawa, S.; Maegawa, T.; Prof, Y.K. Facile and clean oxidation of alcohols in water using hypervalent iodine (III) reagents. *Angew. Chem. Int. Ed.* **2000**, *39*, 1306–1308. [CrossRef]
9. Könning, D.; Olbrisch, T.; Sypaseuth, F.D.; Tzschuckea, C.C.; Christmann, M. Oxidation of allylic and benzylic alcohols to aldehydes and carboxylic acids. *Chem. Commun.* **2014**, *50*, 5014–5016. [CrossRef]
10. Gao, W.; Li, S.; Pal, M.; Liu, Y.; Wan, X.; Li, W.; Wang, S.; Wang, C.; Zheng, G.; Zhao, D. Capping agent-free highly dispersed noble metal nanoparticles supported in ordered mesoporous carbon with short channels and their catalytic applications. *RSC Adv.* **2016**, *6*, 61064–61072. [CrossRef]
11. Pai, Z.P.; Kochubey, D.I.; Berdnikova, P.V.; Kanazhevskiy, V.V.; Prikhod'ko, I.Y.; Chesalov, Y.A. Structure and properties of tungsten peroxopolyoxo complexes-promising catalysts for organics oxidation. I. structure of peroxocomplexes studied during the stepwise synthesis of tetra(diperoxotungsten)phosphate-tetra-n-butyl ammonium. *J. Mol. Catal. A Chem.* **2010**, *332*, 122–127. [CrossRef]
12. Sloboda-Rozner, D.; Witte, P.; Alsters, P.L.; Neumann, R. Aqueous biphasic oxidation: A water-soluble polyoxometalate catalyst for selective oxidation of various functional groups with hydrogen peroxide. *Adv. Synth. Catal.* **2004**, *346*, 339–345. [CrossRef]
13. Saisaha, P.; Buettner, L.; Meer, M.V.; Hage, R.; Feringa, B.L.; Browne, W.R.; Boer, J.W. Selective catalytic oxidation of alcohols, aldehydes, alkanes and alkenes employing manganese catalysts and hydrogen peroxide. *Adv. Synth. Catal.* **2013**, *355*, 2591–2603. [CrossRef]
14. Seth, S.; Jhulki, S.; Moorthy, J.N. Catalytic and chemoselective oxidation of activated alcohols and direct conversion of diols to lactones with in situ-generated bis-IBX catalyst. *Eur. J. Org. Chem.* **2013**, *2013*, 2445–2452. [CrossRef]
15. Mirza, M.; Tavana, M.M.; Boukherroub, R. Oxone/iron (II) sulfate/graphite oxide as a highly effective system for oxidation of alcohols under ultrasonic irradiation. *Tetrahedron Lett.* **2014**, *55*, 342–345. [CrossRef]
16. Gowda, R.R.; Chakraborty, D. Ceric ammonium nitrate catalyzed oxidation of aldehydes and alcohols. *Chin. J. Chem.* **2011**, *29*, 2379–2384. [CrossRef]
17. Das, R.; Chakraborty, D. Cu (II) bromide catalyzed oxidation of aldehydes and alcohols. *Appl. Organometal. Chem.* **2011**, *25*, 437–442. [CrossRef]
18. da Silva, M.J.; da Silva, G.R.N.; Sampaio, V.F.C.; Vilanculo, C.B.; Fernandes, S.A.; Teixeira, M.G. One-pot synthesis of benzaldehyde derivatives in $PdCl_2$-catalyzed reactions with H_2O_2 in alcoholic solutions. *Chem. Pap.* **2021**, *75*, 1545–1554. [CrossRef]

19. Masuda, S.; Takano, S.; Yamazoe, S.; Tsukuda, T. Synthesis of active, robust and cationic Au_{25} cluster catalysts on double metal hydroxide by long-term oxidative aging of $Au_{25}(SR)_{18}$. *Nanoscale* **2022**, *14*, 3031–3039. [CrossRef]
20. Tiburcio, E.; Greco, R.; Mon, M.; Ballesteros-Soberanas, J.; Ferrando-Soria, J.; López-Haro, M.; Hernández-Garrido, J.C.; Oliver-Meseguer, J.; Marini, C.; Boronat, M.; et al. Soluble/MOF-supported palladium single atoms catalyze the ligand-, additive-, and solvent-free aerobic oxidation of benzyl alcohols to benzoic acids. *J. Am. Chem. Soc.* **2021**, *143*, 2581–2592. [CrossRef]
21. Zhao, Y.; Yu, C.; Wu, S.; Zhang, W.; Xue, W.; Zeng, Z. Synthesis of benzaldehyde and benzoic acid by selective oxidation of benzyl alcohol with iron (III) tosylate and hydrogen peroxide: A solvent-controlled reaction. *Catal. Lett.* **2018**, *148*, 3082–3092. [CrossRef]
22. Sun, Q.; Dai, Z.; Meng, X.; Xiao, F. Porous polymer catalysts with hierarchical structures. *Chem. Soc. Rev.* **2015**, *44*, 6018–6034. [CrossRef] [PubMed]
23. Sun, Q.; Xiao, F. Porous polymeric catalysts constructed from vinylated functionalities. *Acc. Mater. Res.* **2022**, *3*, 772–781. [CrossRef]
24. Ferreira, G.A.; Loh, W. Planet–satellite nanostructures based on block copolymer-surfactant nanoparticles surface-decorated with gold and silver: A new strategy for interfacial catalysis. *Adv. Mater. Interfaces* **2019**, *6*, 1900348. [CrossRef]
25. Tao, R.; Ma, X.; Wei, X.; Jin, Y.; Qiu, L.; Zhang, W. Porous organic polymer material supported palladium nanoparticles. *J. Mater. Chem. A* **2020**, *8*, 17360–17391. [CrossRef]
26. Yamashina, M.; Sei, Y.; Akita, M.; Yoshizawa, M. Safe storage of radical initiators within a polyaromatic nanocapsule. *Nat. Commun.* **2014**, *5*, 4662. [CrossRef]
27. Boonpangrak, S.; Whitcombe, M.J.; Prachayasittikul, V.; Mosbach, K.; Ye, L. Preparation of molecularly imprinted polymers using nitroxide-mediated living radical polymerization. *Biosens. Bioelectron.* **2006**, *22*, 349–354. [CrossRef]
28. Huang, Z.; Liu, K.; Liu, M.; Yun, J.; Dong, J.; Chen, Z.; Xie, Z.; Pan, X. Photocatalytic metal-free radical hydrosilylation for polymer functionalization. *Chin. J. Chem.* **2023**, *41*, 2275–2281. [CrossRef]
29. Ben, T.; Ren, H.; Ma, S.Q.; Cao, D.; Lan, J.; Jing, X.; Wang, W.; Xu, J.; Deng, F.; Simmons, J.M.; et al. Targeted synthesis of a porous aromatic framework with high stability and exceptionally high surface area. *Angew. Chem. Int. Ed.* **2009**, *48*, 9457–9460. [CrossRef]
30. Tian, Y.; Zhu, G. Porous aromatic frameworks (PAFs). *Chem. Rev.* **2020**, *120*, 8934–8986. [CrossRef]
31. Wang, Q.; Chen, Q.; Zhao, R.; Wang, H.; Diao, W.; Cui, F.; Li, S.; Wang, H.; Zhu, G. Salen-based porous aromatic frameworks with multi-active sites as anode materials for lithium-ion batteries. *J. Colloid Interface Sci.* **2023**, *648*, 616–622. [CrossRef] [PubMed]
32. Kumar, P.; Das, A.; Maji, B. Phosphorus containing porous organic polymers: Synthetic techniques and applications in organic synthesis and catalysis. *Org. Biomol. Chem.* **2021**, *19*, 4174–4192. [CrossRef]
33. Bayne, J.M.; Fasano, V.; Szkop, K.M.; Ingleson, M.J.; Stephan, D.W. Phosphorous(V) Lewis acids: Water/base tolerant P_3-trimethylated trications. *Chem. Commun.* **2018**, *54*, 12467–12470. [CrossRef] [PubMed]
34. Huang, Y.; Ding, M.; Ding, J.; Kang, J.; Yan, Z.; Zhao, P.; Zhou, X.; Jin, Y.; Chen, S.; Xia, C. Targeted synthesis of a high-stability cationic porous aromatic framework for highly efficient remediation of $^{99}TcO_4^-$. *Chem. Eng. J.* **2022**, *435*, 134785. [CrossRef]
35. Tian, Y.; Song, J.; Zhu, Y.; Zhao, H.; Muhammad, F.; Ma, T.; Chen, M.; Zhu, G. Understanding the desulphurization process in an ionic porous aromatic framework. *Chem. Sci.* **2019**, *10*, 606–613. [CrossRef] [PubMed]
36. Moghaddam, M.; Abbassi, A.; Ghazanfarian, J.; Jalilian, S. Investigation of microstructure effects on performance of hierarchically structured porous catalyst using a novel pore network model. *Chem. Eng. J.* **2020**, *388*, 124261. [CrossRef]
37. Sun, Y.; Zhang, C.; Zhu, X.; Dong, L.; Sun, X. Mass and heat transfer of pressure swing adsorption oxygen production process with small adsorbent particles. *Processes* **2023**, *11*, 2485. [CrossRef]
38. Hyodo, M.; Iwano, H.; Kasakado, T.; Fukuyama, T.; Ryu, I. Using high-power UV-LED to accelerate a decatungstate-anion-catalyzed reaction: A model study for the quick oxidation of benzyl alcohol to benzoic acid using molecular oxygen. *Micromachines* **2021**, *12*, 1307. [CrossRef]
39. Bamoharram, F.F.; Roshani, M.; Heravi, M.M.; Safaie, S. The catalytic performance of preyssler's anion, $[NaP_5W_{30}O_{110}]^{14-}$, in the oxidation of benzyl alcohols. *Phosphorus Sulfur Silicon Relat. Elem.* **2006**, *181*, 2833–2841. [CrossRef]
40. Neves, P.; Lysenko, A.B.; Gomes, A.C.; Pillinger, M.; Gonçalves, I.S.; Valente, A.A. Behavior of triazolylmolybdenum (VI) oxide hybrids as oxidation catalysts with hydrogen peroxide. *Catal. Lett.* **2017**, *147*, 1133–1143. [CrossRef]
41. Su, H.; Yang, C. Selective oxidation of benzyl alcohol catalyzed by (TEAH)nH_3-n$PW_{12}O_{40}$ and its reaction mechanism. *Chin. J. Catal.* **2014**, *35*, 1224–1234. [CrossRef]
42. Aguinaco, A.; Pocostales, J.P.; García-Araya, J.F.; Beltran, F.J. Decomposition of hydrogen peroxide in the presence of activated carbons with different characteristics. *J. Chem. Technol. Biotechnol.* **2011**, *86*, 595–600. [CrossRef]
43. Mao, D.; Jia, M.; Qiu, J.; Zhang, X.F.; Yao, J. N-doped porous carbon supported Au nanoparticles for benzyl alcohol oxidation. *Catal. Lett.* **2020**, *150*, 74–81. [CrossRef]
44. Jacobson, S.E.; Muccigrosso, D.A.; Mares, F. Oxidation of alcohols by molybdenum and tungsten peroxo complexes. *J. Org. Chem.* **1979**, *44*, 921–924. [CrossRef]
45. Carlo, V.; Marco, R. Oxidative cleavage of 1,2-diols to carboylic acids by hydrogen peroxide. *J. Org. Chem.* **1986**, *51*, 1599–1602. [CrossRef]
46. Noyori, R.; Aokib, M.; Sato, K. Green oxidation with aqueous hydrogen peroxide. *Chem. Commun.* **2003**, *34*, 1977–1986. [CrossRef]
47. Correia, L.M.M.; Soliman, M.M.A.; Granadeiro, C.M.; Balula, S.S.; Martins, L.M.D.R.S.; Pombeiro, A.J.L.; Alegria, E.C.B.A. Vanadium C-scorpionate supported on mesoporous aptes-functionalized SBA-15 as catalyst for the peroxidative oxidation of benzyl alcohol. *Microporous Mesoporous Mater.* **2021**, *320*, 111111. [CrossRef]

48. Shul'pin, G.B.; Kozlov, Y.N.; Nizova, G.V.; Süss-Fink, G.; Stanislas, S.; Kitaygorodskiyc, A.; Kulikovad, V.S. Oxidations by the reagent "O_2–H_2O_2–vanadium derivative–pyrazine-2-carboxylic acid". Part 12.[1] Main features, kinetics and mechanism of alkane hydroperoxidation. *J. Chem. Soc. Perkin Trans.* **2001**, *2*, 1351–1371. [CrossRef]
49. Wu, H.; Zhang, X.; Chen, X.; Chen, Y.; Zheng, X. Preparation, characterization and catalytic properties of MCM-48 supported tungstophosphoric acid mesoporous materials for green synthesis of benzoic acid. *J. Solid State Chem.* **2014**, *211*, 51–57. [CrossRef]
50. Huang, X.; Wang, X.; Tan, M.; Zou, X.; Ding, W.; Lu, X. Selective oxidation of alcohols on P123-stabilized Au-Ag alloy nanoparticles in aqueous solution with molecular oxygen. *Appl. Catal. A Gen.* **2013**, *467*, 407–413. [CrossRef]
51. Rautiainena, S.; Simakova, O.; Guo, H.; Leinoc, A.; Kordás, K.; Murzin, D.; Leskelä, M.; Repo, T. Solvent controlled catalysis: Synthesis of aldehyde, acid or ester by selective oxidation of benzyl alcohol with gold nanoparticles on alumina. *Appl. Catal. A Gen.* **2014**, *485*, 202–206. [CrossRef]
52. Ghadamgahi, S.; Williamson, B.; Golovko, V. Activity of catalysts derived from Au_{101} immobilized on activated carbon. *Catal. Lett.* **2016**, *146*, 1027–1032. [CrossRef]
53. Wang, C.; Jiao, L.; Ji, P. Interfacial synthesis of Co-based ultrathin nanosheets with NaF crystal as template and inducer: Fluorine doped $Co(OH)_2$, porous fluorine doped Co_3O_4, and porous Co_3O_4. *Appl. Surf. Sci.* **2022**, *589*, 152923. [CrossRef]
54. Sarkheil, M.; Lashanizadegan, M.; Ghiasi, M. High catalytic activity of magnetic Fe_3O_4@SiO_2-Schiff base-Co (II) nanocatalyst for aerobic oxidation of alkenes and alcohols and DFT study. *J. Mol. Struct.* **2019**, *1179*, 278–288. [CrossRef]
55. Feng, D.; Dong, Y.; Zhang, L.; Ge, X.; Zhang, W.; Dai, S.; Qiao, Z. Holey lamellar high entropy oxide as ultra-highly active heterogeneous catalyst for solvent-free aerobic oxidation of benzyl alcohol. *Angew. Chem. Int. Ed.* **2020**, *59*, 19503–19509. [CrossRef]
56. Gao, W.; Song, Y.; Jiao, W.; Liu, Y. A catalyst-free and highly efficient approach to ozonation of benzyl alcohol to benzoic acid in a rotating packed bed. *J. Taiwan Inst. Chem. Eng.* **2019**, *103*, 1–6. [CrossRef]
57. Sheldon, R.A.; Wallau, M.; Arends, I.W.C.E.; Schuchardt, U. Heterogeneous catalysts for liquid-phase oxidations: Philosophers' stones or trojan horses? *Acc. Chem. Res.* **1998**, *31*, 485–493. [CrossRef]